Available online at www.sciencedirect.com

ScienceDirect

Proceedings of the Combustion Institute 36 (2017) 543–551

Proceedings of the Combustion Institute

www.elsevier.com/locate/proci

Contributions to improving small ester combustion chemistry: Theory, model and experiments

Daniel Felsmann [a,1], Hao Zhao [b,1], Qiang Wang [b], Isabelle Graf [a], Ting Tan [b], Xueliang Yang [b], Emily A. Carter [b], Yiguang Ju [b], Katharina Kohse-Höinghaus [a,*]

[a] *Department of Chemistry, Bielefeld University, Universitätsstraße 25, D-33615 Bielefeld, Germany*
[b] *Department of Mechanical and Aerospace Engineering, Princeton University, Princeton, NJ 08544, USA*

Received 26 November 2015; accepted 25 May 2016
Available online 11 June 2016

Abstract

Biodiesel combustion models demand detailed understanding of the reactions undertaken by the ester functional group in the molecule. Investigations of the chemistry of small methyl esters can contribute to this goal. We have thus chosen methyl propanonate (MP) as a representative ester molecule in a study combining theory, model, and experiments. As an advantage, its reactions are also amenable to high-level theoretical calculations. Based on recent theoretical calculations (Tan et al., 2015), a new kinetics model for small ester combustion was developed and validated. New experimental results were obtained here in an extensive range of conditions, including full speciation in laminar low-pressure flames at two different stoichiometries ($\phi = 0.8$ and 1.5) using electron ionization (EI) molecular-beam mass spectrometry (MBMS) and flame speed measurements in a spherical confined chamber (1–6 atm). Comparison of the experimental data to the present model shows overall improved performance. Some specific new reaction pathways to form methanol, methylketene, methyl acetate, and acetic acid from the fuel radicals were identified and will permit more detailed insights into the combustion properties of methyl propanoate.

Keywords: Methyl propanonate; Kinetic model; Low-pressure flame; Flame speed; Molecular-beam mass spectrometry

1. Introduction

Biofuels have received increasing attention in the attempt to develop more sustainable transportation strategies because of their renewable nature and perceived potential to reduce carbon dioxide and soot emissions [1,2]. The main biofuels used today are ethanol and biodiesel, and the combustion chemistry of biofuels has been the focus of recent research reviews [3,4]. Biodiesel commonly consists of a mixture of saturated and unsaturated long-chain ($\sim C_{12}$–C_{22}) mono-methyl- and -ethyl esters developed from

* Corresponding author. Fax: +49 5211066027.
E-mail addresses: yju@princeton.edu (Y. Ju), kkh@uni-bielefeld.de (K. Kohse-Höinghaus).
[1] These authors contributed equally to the work.

http://dx.doi.org/10.1016/j.proci.2016.05.012
1540-7489

transesterification of animal fats and plant oils [4,5]. Several previous investigations have focused on long-chain esters [6,7]; it was found that the ester functional group affects the fuel oxidation and formaldehyde formation at low temperature. Therefore, detailed knowledge of the reaction kinetics of the methyl ester functional group remains central to provide specific insight into the chemistry distinctive to methyl esters.

More profound knowledge about the reaction kinetics enabled by the ester functional group present also in the larger molecules in biodiesel can be achieved by investigating methyl esters with shorter chains of C_1–C_4, namely methyl formate (MF), methyl acetate (MA), methyl propanoate (MP), and methyl butanoate (MB). The short side chains of these small esters allow the investigation of unique pathways to form CH_2O and methanol arising from the low bond dissociation energies of the C–C and C–O bonds next to the ester functional group. Such knowledge needed to improve the combustion kinetics for small ester molecules can then be used also in mechanisms for the more relevant larger esters in biodiesel. Extensive combustion results for MF, MA, and MB have been presented already in the literature [8–12]. Diffusion flame extinction measurements [7] showed that MP has a different fuel reactivity from other small methyl esters. Unfortunately, kinetic studies for MP remain scarce. Recently, the ignition of MP was studied using reflected shock waves [13], and the results were compared with existing models developed from similarity rules of molecular structures. Moreover, laminar flame speeds of MP were measured at atmospheric pressure [14] and MP low-pressure flame studies were also reported [15]. Recently, a comparative pyrolysis study of methyl and ethyl propanoate included numerical simulations and shock tube measurements at elevated temperatures and 1.5 atm [16]. Furthermore, theoretical calculations were recently performed on the H-abstraction by OH [17] and H-abstraction reactions at the methoxy group of methyl esters [18]. Recent high-level quantum chemistry and kinetics computations have addressed the decomposition and isomerization of MP radicals [19]; also, H-abstractions from MP by H/O/OH/CH_3/HO_2 have been calculated [20]. These newly calculated reaction rates and their pressure dependences deviate significantly from those estimated from the similarity rules. However, only a few measurements of species concentrations in flames and flame speeds at elevated pressure are available. It is unclear how the change in predicted reaction rates and pathways will affect MP oxidation in flames.

In the present study, based on the knowledge of high-level theoretical calculations of MP reactions [19,20], our goal is to obtain new measurements of species distribution in low-pressure flames and flame speeds at elevated pressure, and to develop a new kinetics mechanism to gain detailed insights into the reaction kinetics of MP. Specifically, full speciation measurements of MP oxidation at 40 mbar were made at two different stoichiometries ($\phi = 0.8$ and 1.5) using low-pressure flat flames. Flame speed measurements were carried out at atmospheric and elevated pressures up to 6 atm. A new MP mechanism then was developed using the new rate constants for unimolecular dissociation and isomerization kinetics of MP radicals, as well as H-abstraction reactions from MP by H/O/OH/CH_3/HO_2 determined by ab-initio calculations, incorporating our recent methyl acetate mechanism [10]. To examine the predictive capability of the model within a broad range of conditions, the model was compared to the new species and flame speed measurements in this study as well as existing datasets in the literature [14,15,21].

2. Ab-initio reaction rate calculations and kinetics modeling

Previously, we developed a successful methyl acetate mechanism [10] using a combination of high-level quantum chemistry, kinetics computations, and experimental measurements. By contrast, the few existing theoretical and experimental studies of MP decomposition [21] and H-abstraction by OH [17,22] and HO_2 [23] exhibit large discrepancies between theory [17] and experiments [22] for H-abstraction rates by OH and in species profiles of MP pyrolysis [21].

Therefore, high-level ab-initio RRKM master-equation calculations using the VARIFLEX code [24] were performed to determine rate coefficients for H-abstractions from MP by H, CH_3, OH, HO_2, and O [20] and for subsequent unimolecular reactions of the three MP radicals produced from H-abstraction [19]. The asymmetric Eckart approximation was employed to account for quantum tunneling in all kinetics calculations. Details of the calculations are available in [19,20]. Figure S1 and Table S1 schematically represent important reactions included in this work, while Fig. S2 shows an example that the use of reaction rates from similarity rules can lead to inconsistent results. Specifically, rovibrational properties of all studied critical points were determined at the DFT-M08-HX/cc-pVTZ level of theory [25]. For the H-abstraction reactions from MP, the stationary point energies were then refined at the CCSD(T)/cc-pVXZ (X = D,T,Q) level [26]. The energy extrapolation [27] to the complete basis set (CBS) limit using the energies with the cc-pVDZ, cc-pVTZ basis sets, referred to as CBS(D–T), are in good agreement with the corresponding CBS limit using the cc-pVTZ and cc-pVQZ bases (CBS(T–Q)) for the reactions MP+H/O/OH/CH_3/HO_2. For consistency

with other methods used in [19], the former CBS extrapolation was used in the kinetics calculations for all five studied abstraction reaction systems. Rate constants for MP H-abstraction by H, CH_3, and O were obtained using (E, J)-resolved TST-RRKM theory within the one-dimensional (1D) separable-hindered-rotor approximation for all torsions, where the rotational potential energy surface (PES) for the low-frequency torsional mode was obtained by a relaxed surface scan at the DFT-M08-HX/cc-pVTZ level. For MP H-abstraction by OH and HO_2, the ring-like structures of transition states suggest strong coupling between the internal rotations, so the multi-structure all-structure (MS-AS) method [28] was applied to predict partition functions of both reactants and transition states in MP+OH/HO_2 reaction systems. In the MS-AS method, all distinguishable conformers were expected to contribute to the total partition function according to Boltzmann weighting, the structures and relative energies of which were obtained using DFT-M08-HX/cc-pVTZ. The predicted partition functions were then utilized to obtain rate constants using canonical TST. Figure S3 depicts the predicted total H-abstraction rate of MP by OH compared to literature reports, which clearly demonstrates the success of the current approach.

Regarding unimolecular reactions for MP radicals, the PES was obtained at the CCSD(T)/CBS(T-Q)//DFT-M08-HX/cc-pVTZ level. Multi-well multi-channel RRKM/master equation [29] calculations were employed to obtain temperature- and pressure–dependent rate coefficients within the 1D separable-hindered-rotor approximation for all torsions. The details for these calculations can be found in [19].

With these newly predicted rates, a new MP model was developed based on our previous studies on methyl acetate [10] and acetylene [30] (to include species beyond C_3). There was no attempt to optimize the rates to fit any particular experiments. The CHEMKIN software [31] was used in numerical simulations. Multicomponent molecular diffusion and Soret diffusion are included in the simulation calculation. Normalized gradient and curvature tolerances were set to 0.02 to obtain converged solutions.

3. Experimental methods

3.1. Flame speed measurements

Flame speed experiments were conducted at Princeton University in a heated, high-pressure constant-volume spherical chamber. The chamber was housed in a temperature-controlled oven. Liquid methyl propanoate was vaporized at 400 K in a separated vaporizer before filling the spherical chamber through electrically heated lines. The mixture compositions were prepared by using the partial pressure method. The initial pressure was varied from 1 to 6 atm. For each case, the helium concentration was adjusted to control Lewis number and flame temperature to prevent ignition difficulty, excessive thermal expansion, cellular instability, buoyancy effects, and extrapolation errors. Experimental conditions are shown in Table S2. The quiescent combustible mixture was centrally ignited. The unsteady flame propagation speed was quantified directly using high-speed Schlieren imaging at frame rate of 8000. Details of the apparatus, procedures of flame speed extraction, and experimental uncertainties are described elsewhere [32,33]. In brief, smoothed flame-radius vs. time-history data was collected in an automated flame-edge detection and circle-fitting program. The unstretched flame speeds relative to the burned gas, Sb_0, were calculated using the nonlinear extrapolation method by Chen [34], and this extrapolated flame velocity can be converted to the un-stretched propagation speed relative to the unburned gas, Su_0, using the calculated density ratio [31]. Uncertainties in the flame speeds were calculated from the root-mean-square sum of the uncertainties in the flame-radius measurement and initial conditions.

3.2. Low-pressure flame experiments

Low-pressure flame experiments were performed at Bielefeld University using an EI-MBMS instrument described earlier [35]. In short, laminar premixed MP flames were stabilized on a moveable water-cooled flat bronze burner with a matrix diameter of 65 mm. The liquid fuel was supplied by a syringe pump and evaporated at 400 K and 600 mbar in the evaporation vessel, while gases were metered by calibrated mass-flow controllers using appropriate gas conversion factors. Two conditions with a cold gas velocity of 72.96 cm/s (at 333 K and 40 mbar) were chosen; a fuel-rich flame ($\phi = 1.5$; molar percentages of 11.5% MP/ 38.5% O_2/ 50% Ar) and a fuel-lean flame ($\phi = 0.8$; 6.9% MP/ 43.1% O_2/ 50% Ar).

To determine quantitative species profiles, gas samples were extracted from the flame via a quartz nozzle (300 μm diameter, 25° opening angle) and further expanded into a first pumping stage ($\sim 10^{-4}$ mbar). The formed molecular beam was guided through a skimmer into the ionization region where molecules were ionized by a pulsed EI source; resulting ions were detected by a reflectron time-of-flight MBMS with a mass resolution of ~4000.

Quantification followed established routines and calibration procedures [35,36]. For major species mole fractions, the elemental balance of C, O, and H was taken into account resulting in an uncertainty of ~20%. For intermediate species, direct calibration measurements were performed when possible with an associated uncertainty of ~30%. All other intermediate

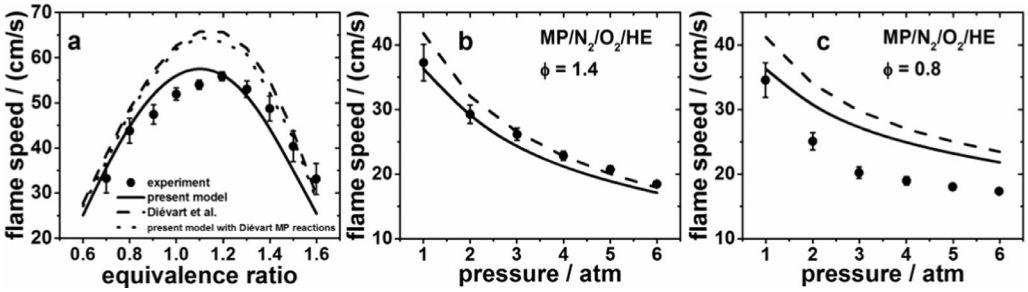

Fig. 1. Laminar flame speed of mixtures of (a) MP/air at 1 atm, 400 K, and variable equivalence ratio; (b) MP/N_2/O_2/He at $\phi = 1.4$; and (c) $\phi = 0.8$ for elevated pressures. Symbols: experiment, lines: present model, dashed lines: DM [7], dotted line: present model with DM [7] MP reactions.

quantifications rely on the relative-ionization-cross-section method (RICS) [37] or convolution of literature ionization cross sections with the known energy distribution of the ionizing electrons [35], resulting in estimated uncertainties of factors 2–4.

Flame temperature profiles (given in Fig. S6) were obtained from the pressure in the first pumping stage following [38] and calibrated at a height $h = 20$ mm in the exhaust by OH planar laser-induced fluorescence, excited in the ($A^2\Sigma^+ - X^2\Pi$, 1-0) band in the range of 282.6–282.7 nm with a dye laser pumped by a Nd:YAG laser. Detection was performed with a combination of a monochromator and an intensified camera as described in [10]. Temperatures of 2167 K ($\phi = 1.5$) and 1890 K ($\phi = 0.8$) at $h = 20$ mm resulted with an uncertainty of $\pm$ 50 K.

4. Results and discussion

4.1. Flame speeds at elevated pressures

Figure 1 shows the comparison of predicted and measured flame speeds for MP/air mixtures at variable equivalence ratio and for MP/N_2/O_2/He mixtures at elevated pressures, respectively. It is observed that the present model predicts the flame speed dependence on equivalence ratio and pressure much better than the Diévart et al. [7] model (here abbreviated as DM), developed mainly from the similarity rule, especially for mixtures in air and for the rich condition (Fig. 1a and b).

For MP/air combustion, the flame speed at atmospheric pressure and 400 K reaches a maximum of 56 cm/s near $\phi = 1.2$. The overall trend is well predicted by the present model within $< 10\%$, while the DM model over-predicts the flame speed in a broad range of equivalence ratios. Using our new model and replacing the new sub-mechanism for MP decomposition with the MP reactions of DM shows no significant change in the prediction of the flame speed compared to the original DM model. Therefore the improved predictability of our model can clearly be attributed to the high-level theoretical rate calculations of H-abstractions of MP and the subsequent decomposition of MP radicals, which play an essential role in MP consumption and intermediate species production. Figure 1b and c show that the MP flame speed decreases rapidly with an increase of pressure. For the rich case (Fig. 1b), the measured and predicted flame speeds agree well. However, for the lean case (Fig. 1c) both models significantly over-predict the flame speeds at elevated pressure by 20–35%, which is much larger than the experimental uncertainty (~5%) that arises from fuel concentration, flame instability, ignition kernel shape, and the extrapolation method. Although the new model predicts the flame speed slightly better than DM, both models fail to capture the pressure dependence, demonstrating that some uncertainties still remain for lean combustion at elevated pressure. Specifically, at higher pressure the uncertainty from the fuel concentration becomes smaller and no serious flame instability was observed experimentally. Moreover, at higher pressure the Markstein length decreases, corresponding to lower uncertainty from flame speed extrapolation. Therefore the difference between experiment and prediction at higher pressure should mainly reflect the uncertainty of the model.

Sensitivity analyses were conducted for rich and lean cases at 1 and 6 atm using the present model (Fig. S4). The results show that the flame speed is controlled by chemistry of small species at both conditions. The flame speed at rich conditions is dominated by the two competing reactions $H+O_2 \rightarrow O+OH$ (R_1) and $CH_3+H(+M) \rightarrow CH_4(+M)$ (R_2). R_1 is the major branching reaction at high temperature, and R_2 is the main termination reaction at fuel-rich conditions because of large mole fractions of CH_3 and H. With the small uncertainties of these two reactions, the rich flame speed is well predicted by both models. However, for the fuel-lean condition, with larger O_2 and OH concentrations, the termination reaction $H+O_2(+M) \rightarrow HO_2(+M)$

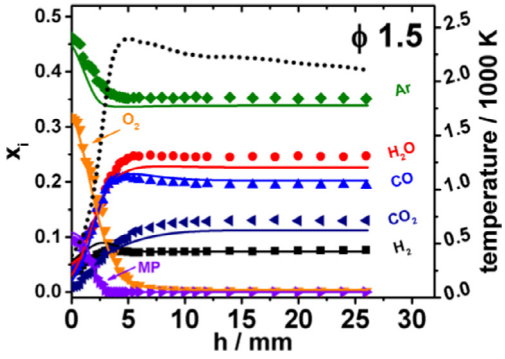

Fig. 2. Major species mole fractions in the fuel-rich MP flame and the measured temperature profile (dotted line, right axis). Symbols: experiment, lines: present model.

(R_3) tends to be more important than R_2. The sensitivity analysis shows that the competing reactions R_1 and R_3 as well as CO+OH⇌CO_2+H dominate the flame speed. Furthermore, the competing pairs HCO+O_2→CO+HO_2 (R_4) and HCO(+M)→H+CO(+M) (R_5) as well as CH_3+H(+M)→CH_4(+M) (R_2) and CH_3+HO_2→CH_3O+OH (R_6) also affect the flame speed. R_4 and R_5, recently investigated by Santner et al. [39], have relatively higher uncertainties which may cause the discrepancies in the lean case. Note that the change of MP decomposition rates has only small effect on the predicted flame speeds in the sensitivity analysis, implying that the current model may still have uncertainties in small species reactions such as C_3H_5O and $C_2H_3O_2$ after MP radical decomposition at elevated pressure.

4.2. Combustion chemistry of MP in flat low-pressure flames

The current model was also tested for speciation under low-pressure conditions, using premixed flames of MP at $\phi = 1.5$ and 0.8, and compared to the widely recognized models of Diévart et al. [7], DM, and Yang et al. [15] (here abbreviated as YM). Only the fuel-rich case is shown here; the fuel-lean flame data are presented in the Supplemental material (Figs. S7–S11) along with a table of all quantified species including their calibration method, electron energy, and literature ionization threshold (Table S3).

Figure 2 shows the main species (MP, O_2, Ar, CO, CO_2, H_2 and H_2O) mole fraction profiles along with the predictions from the present model, calculated with the given temperature profile as a function of the height above the burner, h. Most species profiles and their burnt gas values are reasonably well predicted with some noted discrepancies (~2%) for H_2O and CO_2 that can potentially be attributed to the neglect of OH (~2% mole fraction) in the main species evaluation or the uncertainty in the temperature.

Figure 3 shows the reaction path flux for MP oxidation for $\phi = 1.5$ at $h = 2.5$ mm corresponding to a temperature of 1370 K where most intermediates show their maximum mole fractions.

MP is mainly consumed by H-abstractions from H, OH, and O, leading to three different radicals: $CH_2OCOC_2H_5$, $CH_3OCOCHCH_3$, and $CH_3OCOCH_2CH_2$ (25.2%, 33.2%, and 35.9%); 14.4% of $CH_3OCOCHCH_3$ isomerizes to $CH_2OCOC_2H_5$.

The three fuel radicals decompose mainly by β-scission to CH_2O+C_2H_5CO (44.0% of the fuel) and C_2H_4+CH_3OCO (42.1% of the fuel), and indeed, the highest mole fractions produced in the flame were detected for CH_2O and C_2H_4 (8.0×10^{-3} and 1.8×10^{-2}). Figure 4(a–d) accordingly shows the mole fraction profiles of CH_2O, C_3H_5O, C_2H_4, and $C_2H_3O_2$ along with the modeling results; note that the EI-MBMS detection doesn't permit us to identify the structures of C_3H_5O, and $C_2H_3O_2$.

The comparison demonstrates the excellent predictive capability of the present model for these species. The predicted mole fractions of the primary stable species CH_2O and C_2H_4 (Fig. 4a and c) are in very good agreement with the measurements, better than the other two literature models. Regarding the corresponding radicals from the first β-scission reactions, C_3H_5O and $C_2H_3O_2$ (Fig. 4b and d), these exist at much lower concentrations due to their high reactivity, and their quantification is only achieved within a factor of 2–4. C_3H_5O (Fig. 4b) is severely under-predicted by all models (by ~20× for the present model and YM and ~45× for DM); note also the interesting shape. In the present model, both possible isomers CH_3COCH_2 and C_2H_5CO are represented, enabling better reproduction of the experimental profile shape. $C_2H_3O_2$ (Fig. 4d) decomposes to CO_2+CH_3 very fast; it is not included in the model of Diévart et al. [7] and severely under-predicted (by ~10^3×) by Yang et al. [15], while the present model shows an appreciable performance predicting it as CH_3OCO.

Figure 4e provides the mole fraction for methanol CH_3OH (maximum 8.6×10^{-4}), best predicted by the present model, while DM and YM under-predict the mole fraction by factors of ~2 and ~8, respectively, a considerable deviation for a stable species. Methanol, together with methylketene, is identified to be a product from the fuel radical $CH_3OCOCHCH_3$ via the H-association reaction $CH_3OCOCHCH_3$+H which leads to the highly vibrationally excited species $CH_3OCOCH_2CH_3^*$ that decomposes very quickly to CH_3OH+CH_3CHCO, in analogy to our recent findings for MA [10]. In the schematic diagram in Fig. S1b, this reaction sequence is labeled as D.

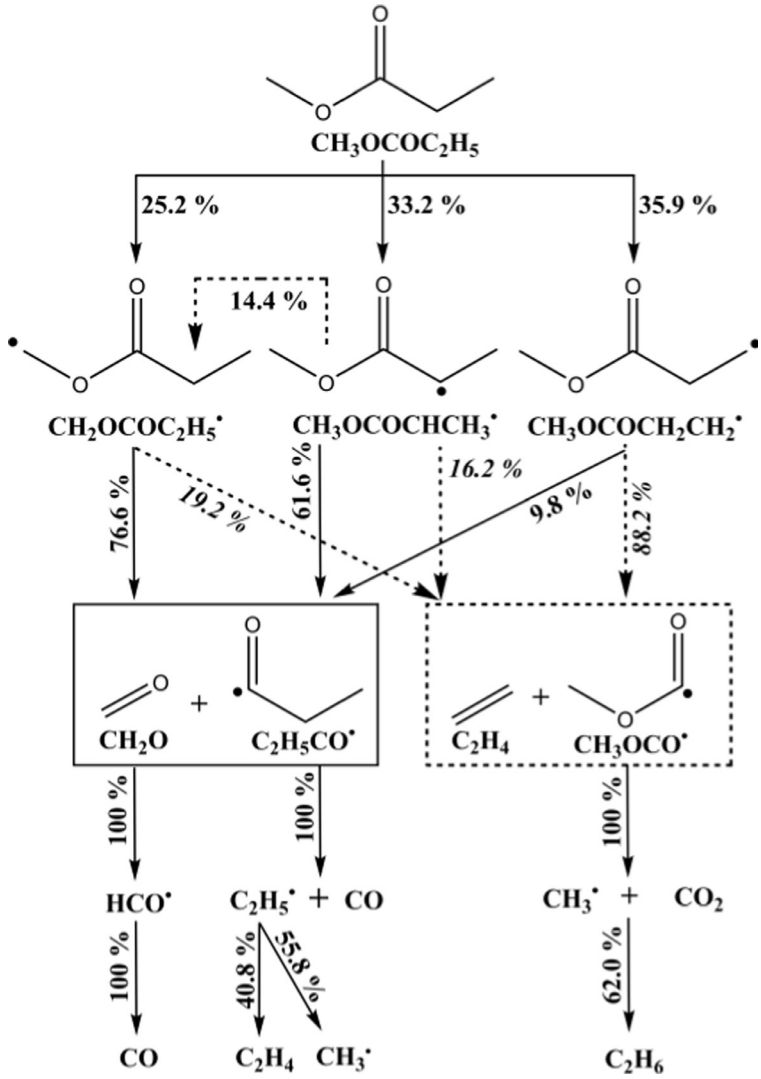

Fig. 3. Reaction pathway analysis at 90% fuel consumption showing the net carbon flux for reactants, main intermediates, and products at $\phi = 1.5$, $h = 2.5$ mm, $T = 1370$ K.

This new pathway, not included in the other mechanism, results from the pressure–dependent nature of the association reaction between H and MP radicals and enhances the prediction quality considerably. This reaction sequence is a unique feature in the combustion behavior of MP, since it produces more methanol than the common CH_3+OH $\rightleftharpoons$ CH_3OH.

Figure 4f presents C_3H_4O, assumed to be methylketene and quantified accordingly, as the second product of the aforementioned reaction. The experimental mole fraction of 2.7×10^{-4} is well reproduced by the present model, while DM over-predicts by a factor of ~10 and YM under-predicts by a similar amount. The substantially improved performance of the present model is encouraging and demonstrates the value of the updated rate constants for MP-related reactions.

Further important species in the combustion of MP are CH_3 and C_2H_5, which are produced by C–O bond scission of C_3H_5O and $C_2H_3O_2$. CH_3 then further reacts by radical recombination to CH_4 (~9 %) and by recombination to C_2H_6 (~64 %). Reactions of C_2H_5 lead to the formation of C_2H_2 by consecutive H-abstractions and by H-abstraction and O-addition to ketene (C_2H_2O) via C_2H_3 and CH_2CHO. The results for these species are presented in Fig. 5.

The predictions with the present model show a very good performance, much improved over the

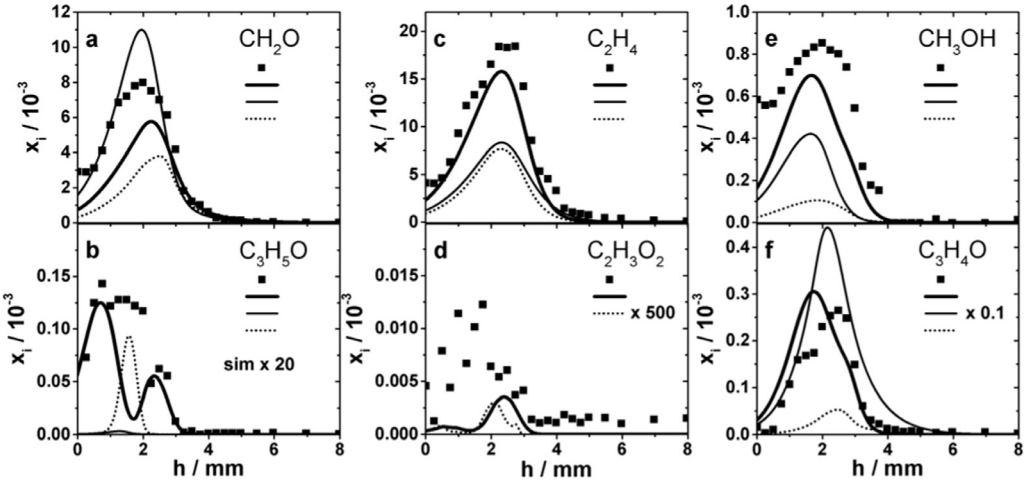

Fig. 4. Mole fraction profiles of first decomposition products for the fuel-rich case. Symbols: experiment, thick lines: present model, thin lines: DM [7], dotted lines: YM [15].

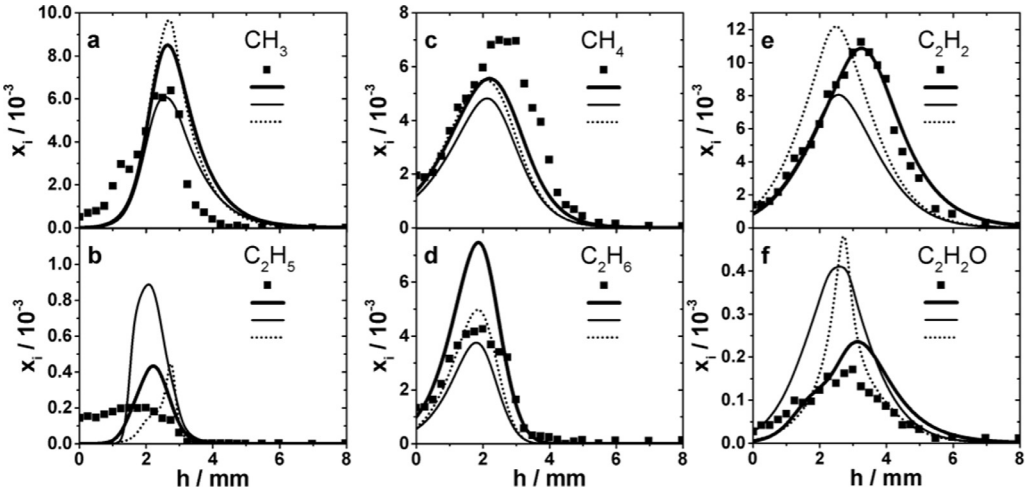

Fig. 5. Mole fraction profiles of CH_3, C_2H_5, CH_4, C_2H_6, C_2H_2, and C_2H_2O for the fuel-rich flame. Symbols: experiment, thick lines: present model, thin lines: DM [7], dotted lines: YM [15].

two literature models, for all species displayed in Fig. 5 except for C_2H_6 with a deviation of less than a factor of 2.

The specific structure of the ester functional group includes two oxygen atoms and therefore an increased tendency to build doubly-oxygenated species even in high-temperature conditions is expected. Indeed, species at masses corresponding to $C_3H_6O_2$ and $C_2H_4O_2$, most likely methyl acetate (CH_3COOCH_3) and acetic acid (CH_3COOH), have been detected in the experiments. A flux analysis with the present model shows a direct pathway from the fuel radical, $H+CH_3OCOCHCH_3 \rightarrow CH_3+CH_2COOCH_3$ (~13 %). CH_2COOCH_3 then reacts to form methyl acetate by H-addition – a termination by combination –, or isomerizes to CH_3COOCH_2; the latter was recently found [10] to produce acetic acid by radical association with CH_3, O, H, or OH and subsequent dissociation even in flame conditions. Figure 6 presents the measured mole fraction profiles of these two species (quantified as methyl acetate and acetic acid).

The present model satisfactorily predicts these profiles (within a factor of ~2 for $C_3H_6O_2$ and ~1.5 for $C_2H_4O_2$), while they are significantly underpredicted by the two literature models.

Overall, the current model is able to predict the majority of species that result from the initial MP radicals in very good agreement with the

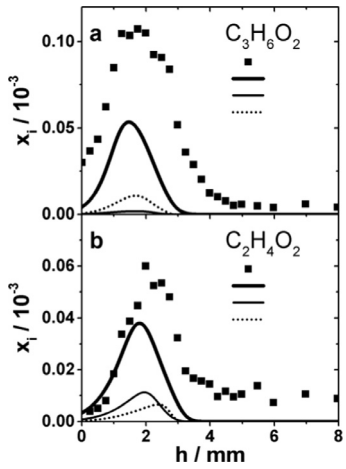

Fig. 6. Mole fraction profiles of $C_3H_6O_2$ and $C_2H_4O_2$; symbols: experiment, thick lines: present model, thin lines: DM [7], dotted lines: YM [15].

experiments. Further validation for the performance of this new model is given in the Supplemental Material, where it is used to simulate the previous flame measurements by Yang et al. [15] (Figs. S12 and S13) and compared to pyrolysis data measured and modeled by Zhao et al. [21] (Fig. S14).

5. Conclusions

In this work, detailed insight into the combustion chemistry of MP has been provided using a combination of experimental and theoretical kinetics studies that cover a wide range of conditions in terms of stoichiometry and pressure. In low-pressure premixed flames at two different stoichiometries, 35 species were quantified, providing an extensive dataset for a critical examination. As a complement, flame speed measurements were provided at atmospheric and elevated pressures at both lean and rich conditions. The experimental results were used to develop a new MP model, based on a previously reported model for MA and extended by recently calculated rate constants for MP radical decomposition and MP H-abstraction. The performance of this new model in comparison with the experimental data demonstrated advanced prediction capability over the complete experimental range in contrast to other/previous MP models. Especially the identification of new reaction pathways led to a substantial improvement compared to previous models not containing these pathways. These include the formation of methanol and methylketene due to H-addition to the $CH_3OCOCHCH_3$ radical and consecutive disproportionation as well as formation of higher oxygenated intermediate species such as methyl acetate and acetic acid.

Acknowledgments

YJ and EAC at Princeton acknowledge the support from the Combustion Energy Frontier Research Center, funded by the United States Department of Energy, Basic Energy Sciences under Award Number De-SC0001198 and U.S. National Science Foundation grants CBET-1507358 (YJ) and CHE/DMR-1265700 (EAC).

Supplementary materials

Supplementary material associated with this article can be found, in the online version, at doi: 10.1016/j.proci.2016.05.012.

References

[1] S. Chu, A. Majumdar, *Nature* 488 (2012) 294–303.
[2] C.K. Westbrook, W.J. Pitz, H.J. Curran, *J. Phys. Chem. A* 110 (2006) 6912–6922.
[3] K. Kohse-Höinghaus, P. Oßwald, T.A. Cool, T. Kasper, N. Hansen, F. Qi, et al., *Angew. Chem. Int. Ed.* 49 (2010) 3572–3597.
[4] C.K. Westbrook, *Ann. Rev. Phys. Chem.* 64 (2013) 201–219.
[5] A. Demirbas, *Prog. Energy Combust. Sci.* 31 (2005) 466–487.
[6] P. Dagaut, S. Gaïl, M. Sahasrabudhe, *Proc. Combust. Inst.* 31 (2007) 2955–2961.
[7] P. Diévart, S.H. Won, J. Gong, S. Dooley, Y. Ju, *Proc. Combust. Inst.* 34 (2013) 821–829.
[8] C.K. Westbrook, W.J. Pitz, P.R. Westmoreland, F.L. Dryer, M. Chaos, P. Osswald, et al., *Proc. Combust. Inst.* 32 (2009) 221–228.
[9] S. Dooley, M.P. Burke, M. Chaos, Y. Stein, F.L. Dryer, V.P. Zhukov, et al., *Int. J. Chem. Kinet.* 42 (2010) 527–549.
[10] X. Yang, D. Felsmann, N. Kurimoto, J. Krüger, T. Wada, T. Tan, et al., *Proc. Combust. Inst.* 35 (2015) 491–498.
[11] S. Gaïl, M.J. Thomson, S.M. Sarathy, S.A. Syed, P. Dagaut, P. Diévart, et al., *Proc. Combust. Inst.* 31 (2007) 305–311.
[12] L. Coniglio, H. Bennadji, P.A. Glaude, O. Herbinet, F. Billaud, *Prog. Energy Combust. Sci.* 39 (2013) 340–382.
[13] Z. Zhang, E. Hu, L. Pan, Y. Chen, J. Gong, Z. Huang, *Energy Fuels* 28 (2014) 7194–7202.
[14] Y.L. Wang, D.J. Lee, C.K. Westbrook, F.N. Egolfopoulos, *Combust. Flame* 161 (2014) 810–817.
[15] B. Yang, C.K. Westbrook, T.A. Cool, N. Hansen, K. Kohse-Höinghaus, *Z. Phys. Chem.* 225 (2011) 1293–1314.
[16] A. Farooq, D.F. Davidson, R.K. Hanson, C.K. Westbrook, *Fuel* 134 (2014) 26–38.
[17] J. Mendes, C.-W. Zhou, H.J. Curran, *J. Phys. Chem. A* 118 (2014) 4889–4899.
[18] Q.-D. Wang, X.-J. Wang, G.-J. Kang, *Comput. Theor. Chem.* 1027 (2014) 103–111.
[19] T. Tan, X. Yang, Y. Ju, E.A. Carter, *Phys. Chem. Chem. Phys.* 17 (2015) 31061–31072.
[20] T. Tan, X. Yang, Y. Ju, E.A. Carter, *Phys. Chem. Chem. Phys.* 18 (2016) 4594–4607.

[21] L. Zhao, M. Xie, L. Ye, Z. Cheng, *Combust. Flame* 160 (2013) 1958–1966.
[22] K.-Y. Lam, D.F. Davidson, R.K. Hanson, *J. Phys. Chem. A* 116 (2012) 12229–12241.
[23] J. Mendes, C.-W. Zhou, H.J. Curran, *J. Phys. Chem. A* 117 (2013) 14006–14018.
[24] S.J. Klippenstein, A.F. Wagner, R.C. Dunbar, D.M. Wardlaw, S.H. Robertson, J.A. Miller, VARIFLEX VERSION 2.02 m, Argonne Natl. Lab. (2010).
[25] Y. Zhao, D.G. Truhlar, *J. Chem. Theory Comput.* 4 (2008) 1849–1868.
[26] K. Raghavachari, G.W. Trucks, J.A. Pople, M. Head-Gordon, *Chem. Phys. Lett.* 157 (1989) 479–483.
[27] D. Feller, D.A. Dixon, *J. Chem. Phys.* 115 (2001) 3484–3496.
[28] J. Zheng, T. Yu, E. Papajak, I.M. Alecu, S.L. Mielke, D.G. Truhlar, *Phys. Chem. Chem. Phys.* 13 (2011) 10885–10907.
[29] J.A. Miller, S.J. Klippenstein, *J. Phys. Chem. A* 110 (2006) 10528–10544.
[30] X. Shen, X. Yang, J. Santner, J. Sun, Y. Ju, *Proc.* Combust. Inst. 35 (2015) 721–728.
[31] R.J. Kee, F.M. Rupley, J.A. Miller, *CHEMKIN II*, Report No. SAND89-8009, Sandia National Laboratories, 1989 and ChemkinPro Reaction design San Diego, 2013.
[32] X. Qin, Y. Ju, *Proc. Combust. Inst.* 30 (2005) 233–240.
[33] J. Santner, F.L. Dryer, Y. Ju, *Proc. Combust. Inst.* 34 (2013) 719–726.
[34] Z. Chen, *Combust. Flame* 158 (2011) 291–300.
[35] M. Schenk, L. Leon, K. Moshammer, P. Oßwald, T. Zeuch, L. Seidel, et al., *Combust. Flame* 160 (2013) 487–503.
[36] A. Lucassen, N. Labbe, P.R. Westmoreland, K. Kohse-Höinghaus, *Combust. Flame* 158 (2011) 1647–1666.
[37] J.C. Biordi, *Prog. Energy Combust. Sci.* 3 (1977) 151–173.
[38] U. Struckmeier, P. Oßwald, T. Kasper, L. Böhling, M. Heusing, M. Köhler, et al., *Z. Phys. Chem.* 223 (2009) 503–537.
[39] J. Santner, F.M. Haas, F.L. Dryer, Y. Ju, *Proc. Combust. Inst.* 35 (2015) 687–694.